https://doi.org/10.5194/acp-2020-831
Preprint. Discussion started: 26 August 2020

Atmospheric Chemistry and Physics Discussions

Laboratory study of the collection efficiency of submicron aerosol particles by cloud droplets. Part I - Influence of relative humidity

Alexis Dépée [1,2], Pascal Lemaitre[1*], Thomas Gelain[1], Marie Monier[2,3], Andrea Flossmann[2,3]

[1] {Institut de Radioprotection et de Sûreté Nucléaire (IRSN), PSN-RES, SCA, Gif-sur-Yvette, France}
[2] {Université Clermont Auvergne, Laboratoire de Météorologie Physique, Clermont-Ferrand, France}
[3] {CNRS, INSU, UMR 6016, LaMP, Aubière, France}
*Correspondence to: Pascal Lemaitre (pascal.lemaitre@irsn.fr)

ABSTRACT

A new In-Cloud Aerosol Scavenging Experiment (In-CASE) has been conceived to measure the collection efficiency (CE) of submicron aerosol particles by cloud droplets. In this setup, droplets fall at their terminal velocity through a one-meter-high chamber in a laminar flow containing aerosol particles. At the bottom of the In-CASE's chamber, the droplet train is separated from the aerosol particle flow - droplets are collected in an impaction cup whereas aerosol particles are deposited on a High Efficiency Particulate Air (HEPA) filter. The collected droplets and the filter are then analysed by fluorescence spectrometry since the aerosol particles are atomised from a sodium fluorescein salt solution ($C_{20}H_{10}Na_2O_5$). In-CASE fully controls all the parameters which affect the CE - the droplets and aerosol particles size distributions are monodispersed, the electric charges of droplets and aerosol particles are controlled, while the relative humidity is indirectly set via the chamber's temperature. This novel In-CASE setup is presented here as well as the first measurements obtained to study the impact of relative humidity on CE. For this purpose, droplets and particles are electrically neutralised. A droplet radius of 49.6 ± 1.3 µm has been considered for six particle dry radii between 50 and 250 nm and three relative humidity levels of 71.1 ± 1.3, 82.4 ± 1.4 and 93.5 ± 0.9 %. These new CE measurements have been compared to the Wang et al. (1978) and the extended model of Dépée et al. (2019) where thermophoresis and diffusiophoresis are implemented. Both models adequately describe the relative humidity influence on the measured CE.

INTRODUCTION

Every year, several billion tons of particulate matter are emitted in the atmosphere, originating mainly from oceans, soils, gas-to-particle conversion, evaporating clouds and from human activities (Jaenicke, 1993). During the last decades, the lifecycle of these aerosol particles (APs) has been a key topic in atmospheric science for many reasons. First, APs play a key role in weather and climate. They act on cloud formation and their chemical composition, size distribution and number concentration affect the droplet size distributions and precipitation (Tao et al., 2012). They also have an impact on the cloud cover which in turn modulates albedo (Twomey et al., 1974) - influencing the Earth's energy budget. Moreover, anthropogenic APs have also been reported causing cardiovascular disorders on humans. In fact, the Great Smog of London in 1952, one of the best-known related events, caused up to 12,000 deaths (Bell et al., 2004). Radioactive material released from a nuclear accident is another AP pollution event. Indeed, many studies revealed that radioactive material like caesium-137 isotopes can attach to the atmospheric APs and were transported over long distances on a continental scale both after the Chernobyl (Devell et al., 1986 ; Jost et al., 1986 ; Pölläen et al., 1997) and the Fukushima (Kaneyasu et al., 2012 ; Adachi et al., 2013) nuclear accidents, respectively in 1986 and 2011. With a half-life up to thirty years, this caesium-137 can remain for decades in the atmosphere - following resuspension cycles of the atmospheric APs - and jeopardise both ecosystems and human survival.

Far away from the source, the main mechanism involved in the AP scavenging originates from the interactions between APs and clouds or their precipitations (Jaenicke, 1993) - referred as the wet

https://doi.org/10.5194/acp-2020-831
Preprint. Discussion started: 26 August 2020

Atmospheric Chemistry and Physics Discussions

deposition. Flossmann (1998) numerically showed that the wet deposition is mainly induced by the in-cloud AP collection since 70 % of the AP mass contained in raindrops reaching the soil comes from the cloud. This result is consistent with the environmental measurements of Laguionie et al. (2014) who evaluated the cloud contribution up to 60 % in the wet AP deposition. The in-cloud AP scavenging is subdivided into two mechanisms - AP activation into cloud hydrometeors and AP collection by clouds hydrometeors. The modelling of the in-cloud AP collection is therefore a fundamental climate, weather and health issue. In most of current AP wet removal models - like DESCAM (Detailed SCAvenging Model, Flossmann, 1985) - the AP collection is described through a microphysical parameter called "collection efficiency" (CE) which quantifies the ability of a droplet to capture the APs present in its surroundings during its fall.

Many microphysical effects influence this CE and their contribution is mainly depending on the AP size. To be collected an AP has to leave the streamline that surrounds the falling droplet to make contact with it. The nanometric AP's motion is affected by the collisions with air molecules - referred as the Brownian diffusion. It results in random movement patterns (see Figure 1, A) which tend to increase the CE when the AP radius decreases. For massive APs, there is an increase of CE as they retain an inertia strong enough to leave the streamline when it curves and to go straight toward the droplet surface - phenomenon called inertial impaction (see Figure 1, B). When considering intermediate AP size, the CE goes through a minimum value called the "Greenfield gap" (Greenfield, 1957) where the AP diffusion and inertia are weaker. In this gap, other microphysical effects can be involved to make the droplet encounter the AP like the interception for instance. It is the collection of APs following a streamline that approaches the droplet within a distance equivalent to the particle radii (a) - see Figure 1, C. Note that the electrostatic forces can have a significant influence on the CE (Tinsley and Zhou, 2015; Dépée et al., 2019). This effect will be discussed in a companion paper (**Dépée et al., 2020**) of this work.

There are also thermophoretic and diffusiophoretic effects which can influence the CE. In clouds, they shall favour the CE increase when evaporation occurs and decrease CE during condensation (due to a thermal equilibrium between the droplet and the air). Thermophoresis exists when a thermal gradient prevails between the air and the droplet. When the relative humidity is below 100 %, the evaporating droplet's surface temperature ($T_{d,s}$) is colder than the bulk air temperature (T_{air}). The average kinetic energy of air molecules is then decreasing when approaching the droplet's surface. An AP is thus attracted by a thermophoretic force near the evaporating droplet (see Figure 1, F) caused by the asymmetry in kinetic energy transferred during each collision. Diffusiophoresis occurs in an environment where a gradient of vapor density in the air exists such as in the surrounding of an evaporating droplet. In this case, water molecules diffuse toward the surrounding air meanwhile the air molecules diffuse toward the droplet surface. In clouds, since the water molar mass is lower than the air molar mass, there is an asymmetry in the momentum transferred to APs close to the evaporating droplet produced by collisions with the molecules from the continuous phase. This diffusion tends to attract the AP to the droplet. Nonetheless, in order to maintain a constant air pressure at the droplet surface, a hydrodynamical flow directed toward the air is induced - this is the Stefan flow. The hydrodynamical drag induced by the Stefan flow tends to repulse APs from an evaporating droplet. The diffusiophoresis is the force resulting from both air and water vapour diffusion, and the Stefan flow which is on average five times larger than the other two ones (Santachiara et al., 2012). Finally, diffusiophoresis repulses APs from the evaporating droplet (see Figure 1, D), decreasing the CE. Since, the thermophoretic process is on average twice larger than the diffusiophoretic one (Tinsley et al., 2006), APs are ultimately attracted toward droplets in a subsaturated air (see Figure 1, E). The coupling of the thermophoresis and diffusiophoresis entails the CE increase when the relative humidity decreases.

The influence of the relative humidity on the CE is described by the well-known Wang et al. (1978) model which is used in many cloud models like DESCAM (Flossmann, 1985). Since their model predicts an important contribution of thermophoresis and diffusiophoresis on the CE for cloud droplet radii (A< 100 µm) and submicron AP radii, it is mandatory to validate those theoretical CEs through experiments. A review of available CE measurements can be found in Ardon-Dryer et al. (2015). The only experimental study that tackles the influence of the relative humidity on the CE for cloud droplets is the one of Ardon-Dryer et al. (2015), which tested two levels of relative humidity of 15 and 88 %. However, in their work they report that the measured electric charge on the droplets were 400 ± 400 elementary charges and on the APs were 1 elementary charge. Therefore, the electrostatic forces should have had a significant influence on the measured CE for the droplet radius considered (A≈ 21.6 µm) as numerically shown by Tinsley and Zhou (2015). Furthermore, there are no equivalent measurements for other cloud droplet sizes neither for high levels of relative humidity as found in-cloud.

https://doi.org/10.5194/acp-2020-831
Preprint. Discussion started: 26 August 2020

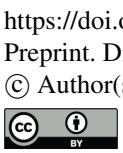

Atmospheric Chemistry and Physics Discussions

The purpose of this work is to fill up the lack of data. Thus, a novel experiment has been developed in order to study the influence of the relative humidity on the CE to assess the magnitude of the thermophoretic and diffusiophoretic processes. With this experiment, the influence of electric charges can also be investigated and this is the object of a companion paper **(Dépée et al., 2020)**. In the first section of this paper, the experimental setup is detailed while the experimental method to evaluate the CE is described in the second one. Finally, the third section is dedicated to the new CE measurements which are presented and compared to theoretical data from the Wang et al. (1978) Eulerian model. Another comparison is made in the last section to the newer Lagrangian model of Dépée et al. (2019) since it can model every microphysical effect involved in the AP collection by cloud droplets (like Brownian motion, inertial impaction, interception, etc.) and specially their coupling. As Dépée et al. (2019) are focusing on the electrostatic forces, the thermophoresis and the diffusiophoresis were not considered. Here, we extend the Dépée et al. (2019) model by adding these phoretic effects. Finally, this study experimentally validates the Dépée et al. (2019) model which provides consistent theoretical CEs for a convenient incorporation in cloud models, pollution models, climate models, and so forth.

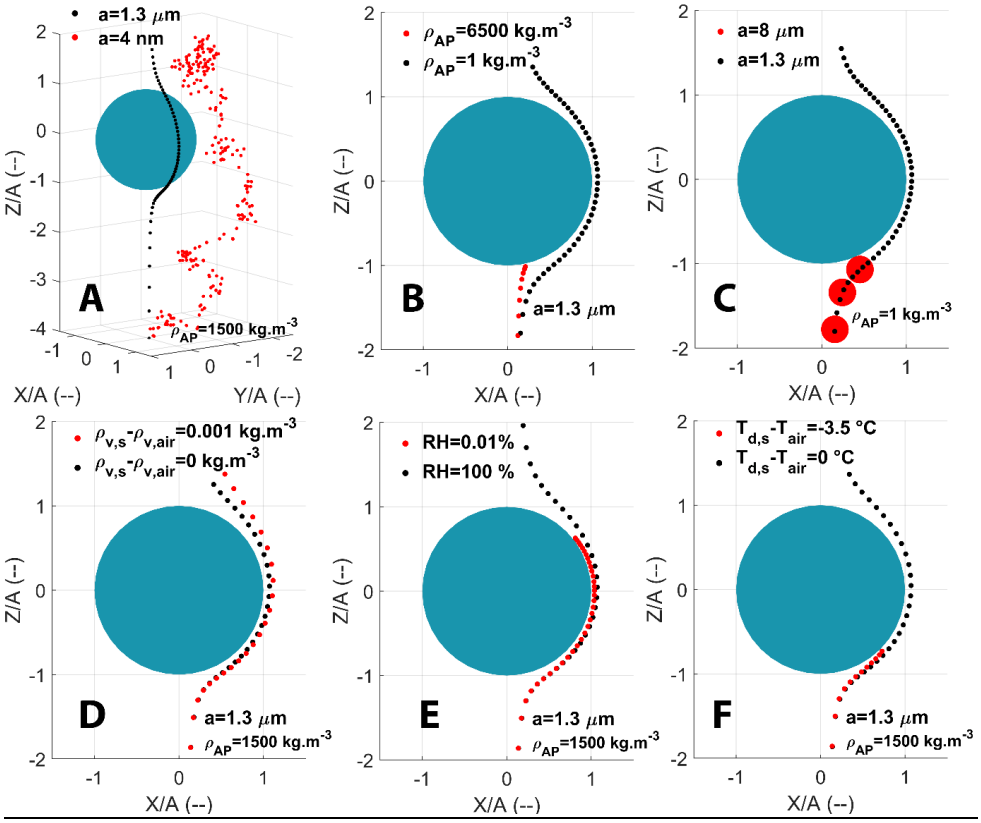

Figure 1 APs trajectories computed with the extended Dépée et al. (2019) model for a 50 µm droplet radius (A) and AP with various radii (a) and densities (ρ_{AP}). The air temperature (T_{air}) and the air pressure (P_{air}) are respectively -17°C and 540 hPa. From Figure 1 A to F, the considered effects are the Brownian motion (A), the inertial impaction (B), the interception (C), the diffusiophoresis (D), the coupling of thermophoresis and diffusiophoresis (E) and the thermophoresis (F) are highlighted. In Figures 1 B, C, E and F - the red trajectories result in an AP collection. In Figure D, the differences in vapor density in the air at the droplet surface ($\rho_{v,s}$) and in the air ($\rho_{v,air}$), equal to 0 and 0.001 kg.m^{-3}, represent an environment with a relative humidity of 100 and 0.01 % respectively. In Figure F, the differences between the temperature at the droplet surface (T_{air}) and in the environment ($T_{d,s}$), equal to 0 and to 3.5°C, represent a relative humidity of 100 and 0.01 % respectively.

https://doi.org/10.5194/acp-2020-831
Preprint. Discussion started: 26 August 2020

Atmospheric Chemistry and Physics Discussions

1 EXPERIMENTAL SETUP

1.1 Overview

All measurements were conducted inside the In-Cloud Aerosol Scavenging Experiment (In-CASE). Figure 2 shows the airflow diagram with the different parts of the experiment in order to study the relative humidity influence on the CE. Note that this In-CASE setup is quite different from the other configuration regarding the electric charges' influence described in the companion paper **(Dépée et al., 2020)**. The major In-CASE's part is the collision chamber (Figure 2) where a laminar flow containing APs interacts with a train of droplets falling at terminal velocity. In this chamber, the droplet and AP size distributions are monodispersed and for this particular work the droplet and AP electric charges are neutralised. In Figure 2, the right side of the diagram shows the AP generation which is described in subsection 1.2. On the left side, an Argon flow is injected into the In-CASE chamber's bottom part to separate droplets from the AP flow - this part is detailed in subsection 1.4.3.1 - meanwhile the AP flow leaves the chamber toward a High Efficiency Particulate Air (HEPA) filter.

The relative humidity in the collision chamber is set through the temperature, this latter being controlled via a cooling system. In the next sections, the droplets and AP characterisation as well as the In-CASE's chamber are detailed.

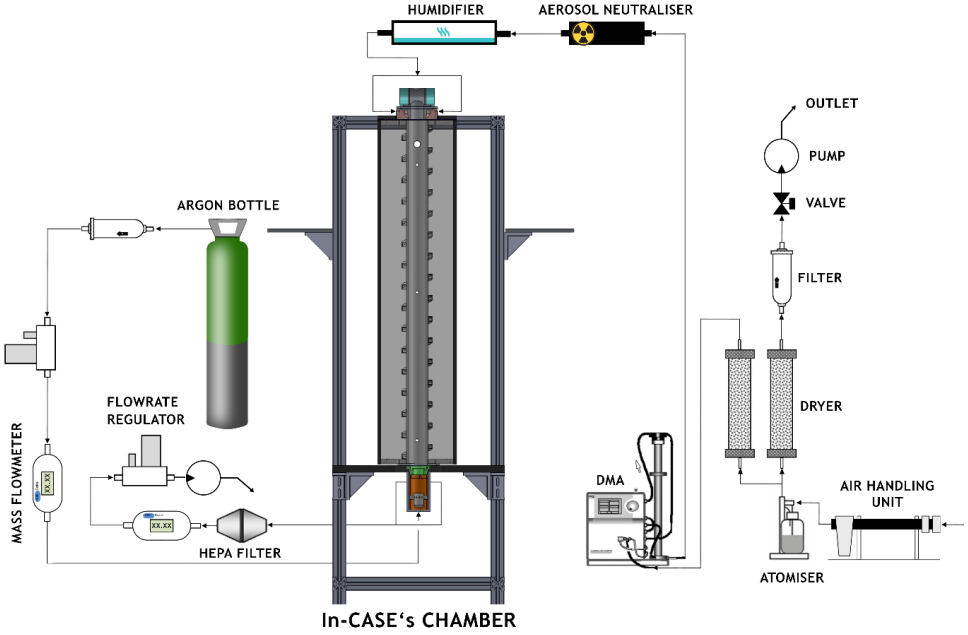

Figure 2 In-CASE setup to study the influence of relative humidity.

1.2 AP generation

APs are generated by the atomisation (atomiser, TSI 3076) of a sodium fluorescein salt solution ($C_{20}H_{10}Na_2O_5$). This molecule has been selected for its significant fluorescent properties, detectable at very low concentrations (down to 10^{-10} g/l). Once atomised, the fine droplets go through a dry diffuser to produce dry APs. In Figure 3, two AP size distributions are presented for two different concentrations of the sodium fluorescein salt solution considered - 36 and 100 g/l - during the experiments. Those two size distributions have been evaluated using a Scanning Mobility Particle Sizer (SMPS). It was observed that the size distribution mode passes from 41 to 67.9 nm in radius when the concentration is three times larger. Since the geometric standard deviation (σ_g) is above 1.75, a Differential Mobility Analyser (DMA; TSI 3080) is used between the atomiser and the In-CASE's

https://doi.org/10.5194/acp-2020-831
Preprint. Discussion started: 26 August 2020

Atmospheric Chemistry and Physics Discussions

chamber to reduce the dispersion of the AP size distribution. After exiting the DMA, the AP flow goes through a low-energy X-ray neutraliser (< 9.5 keV, TSI 3088) so that the AP charge distribution entering the In-CASE's chamber is similar to a Boltzmann distribution. After the neutralisation, the dry AP flow is humidified by a pure water container in order to get high relative humidity in the collision chamber.

Note that, the DMA selects APs according to their electrical mobility - Z in equation (6) - assuming that only single charged APs can leave the DMA. Actually, depending on the AP size distribution and the AP flowrate in the DMA, larger AP radii carrying multiple charges than the one considered can also be selected. Sometimes those multiple charged APs cannot be neglected as discussed in section 2.2.

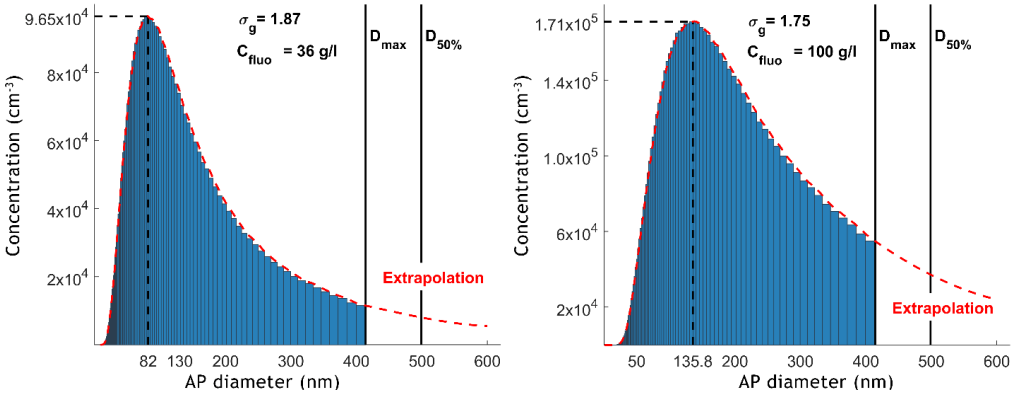

Figure 3 Two typical AP size distributions obtained with a SMPS at the atomiser's outlet. The concentration of the sodium fluorescein salt solution is 36 g/l (**Left**) and 100 g/l (**Right**). D_{max} and $D_{50\%}$ are respectively the maximum diameter selected by the DMA and the cut-off diameter of the impactor at the DMA inlet, at a given AP flowrate (0.6 l/min).

1.3 Droplet characterisation

1.3.1 Droplet generation frequency and size measurement

The droplet generator used for these experiments is a piezoelectric injector provided by Microfab - the MJ-ABL-01 model with an internal diameter of 150 µm. This model has been used for its stability over time, since the experiments can last up to 5 hours. This piezoelectric injector generates droplets - at a given frequency - above their terminal velocity. The distance between two following droplets reduces when droplets fall away from the injector's nozzle since the droplet velocity decreases (see Figure 4, left). It was highlighted during *ex situ* experiments that droplet generation frequencies greater than 25 Hz induce droplet coalescence since the inter-droplet space becomes too short to prevent droplets from aerodynamically disturbing each other. This agrees with Ardon-Dryer et al. (2015) who observed droplet coalescence for droplet generation frequency larger than 30 Hz operating a similar piezoelectric injector. Thus, droplets were generated at 25 Hz in all experiments presented in this current paper.
The droplet generator is placed at the top of the In-CASE's collision chamber, within an injection head (see Figure 6). Few times during an experiment, droplet pictures are recorded by optical shadowgraphy through two facing portholes in the injection head (see Figure 6). A circle Hough transform is then applied to evaluate the droplet radii in the recorded pictures. An example is given in Figure 4 (right) for a 49.7 µm droplet radius. Note that the size distributions of the droplets generated by the piezoelectric injector are considered monodispersed since the droplet size dispersion is very low (σ~1%).

https://doi.org/10.5194/acp-2020-831
Preprint. Discussion started: 26 August 2020

Atmospheric Chemistry and Physics Discussions

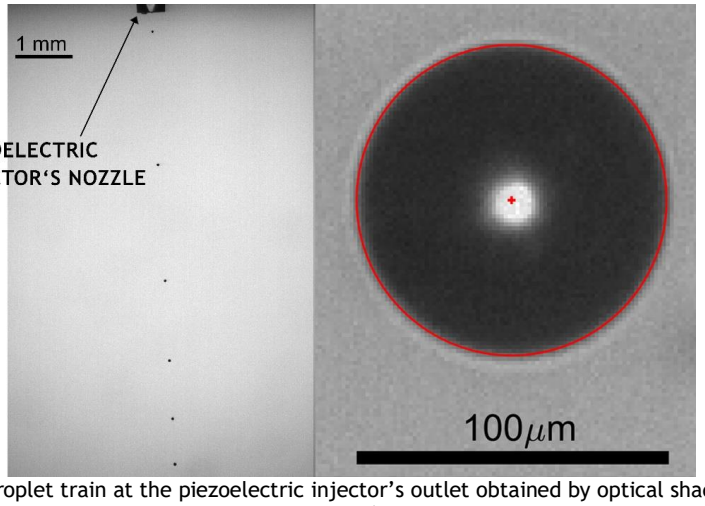

Figure 4 (**Left**) Droplet train at the piezoelectric injector's outlet obtained by optical shadowgraphy - the droplet generating frequency is 200 Hz. (**Right**) A droplet picture obtained by optical shadowgraphy - the droplet radius and centre are detected thanks to a circle Hough transform (red cross and line).

1.3.2 Droplet charge neutralisation

It is well-know that the piezoelectric droplet generator produces highly electrically charged droplets. With a similar device, Ardon-Dryer et al. (2015) measured up to 10^4 elementary charges on the generated droplets. Since this paper focused only on the relative humidity influence, the droplets, as well as APs, must be neutralised.

To do so, an electrostatic inductor was built following Reischl et al. (1977). Two parallel metal plate are placed at the droplet generator's nozzle - this is the electrostatic inductor shown in Figure 5 (labelled 1, left). One plate is connected to a potential (V_{ind}) while the other is connected to the neutral potential - as presented in Figure 5 - in order to induce an electric field (E_{ind}~10^2-10^3 V/m). Sodium chloride is added to the pure water that feeds the piezoelectric injector. According to the generated electric field polarity, the system can selectively attract negative or positive ions toward the nozzle where the droplet is formed. If V_{ind} is positive, the negative chloride ions (Cl^-) migrate toward the nozzle and the positive sodium ions (Na^+) are repulsed from the nozzle and inversely if the potential is negative. Following the electric field amplitude - through V_{ind} - the ion quantity can be set. This system can conclusively control the droplet charge. Note that the sodium chloride concentration has no effect on the principle of induction used here since the ion number is large enough for the entire experiment period (Reischl et al., 1977) - 3.3 g/l has been considered.

To evaluate the droplet charge and then, neutralise the droplets, an *ex situ* experiment has been conducted where the droplet train passed through a capacitor (labelled 2, Figure 5, left). One capacitor's plate is connected to the neutral whereas the other is connected to a high potential (V_{cap}) - inducing an electric field (E_{cap}~10^5-10^6 V/m). A Faraday cage surrounding the capacitor and a plate maintained at a neutral potential are set in order to prevent the electric field at the capacitor (E_{cap}) from disturbing the electric field at the inductor (E_{ind}) which could change the droplet charge. Finally, the potential V_{ind} which electrically neutralises the droplet is found by selecting for the V_{ind} value which minimises the droplet train deflection.

Actually, this system can also be used to precisely evaluated the electric charges on the droplets (for both polarities), this method is applied and presented in **Dépée et al. 2020**.

Note that, the droplet charge induced by the piezoelectric injector has been calculated to -8,400 elementary charges - in line with Ardon-Dryer et al. (2015) using a similar generator. Moreover, after the droplet neutralisation, an uncertainty of 600 elementary charges was evaluated.

https://doi.org/10.5194/acp-2020-831
Preprint. Discussion started: 26 August 2020

Atmospheric Chemistry and Physics Discussions

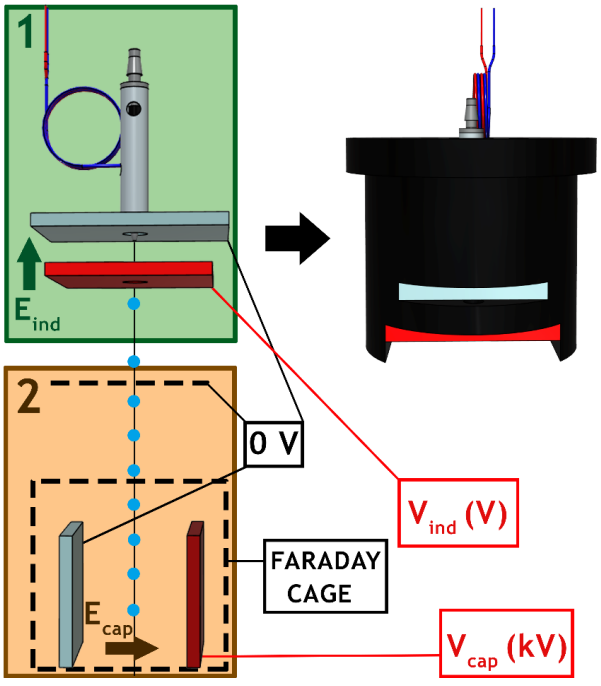

Figure 5 (**Left**) **1** - Electrostatic inductor set at the piezoelectric injector's nozzle to electrically neutralise the droplets. **2** - Capacitor used to check the droplet deviation caused by the electric field in the capacitor (E_{cap}). (**Right**) 3D printing containing the piezoelectric injector and the electrostatic inductor, set in the injection head (see Figure 6).

1.4 In-CASE chamber

The In-CASE chamber (see Figure 2) is subdivided into three stages - the injection head, the collision chamber and the In-CASE chamber's bottom part. These three parts will be detailed in the next subsections.

1.4.1 Injection head

The injection head is composed of two parts - the droplets and the APs injection. The upper part is used to inject the droplets while the APs are inserted in the second part about 10 cm below. This distance is required to measure the droplet size through the two facing portholes (see section 1.3.1) but also to let droplets decelerate and reach their terminal velocity.
The droplet train is injected through a 3D printing set at the top of the droplet injector (see Figure 6). This 3D printing has been constructed to precisely place the droplet generator and the electrostatic inductor together (see Figure 5, right). Indeed, the electrostatic inductor has to keep the same position relative to the droplet generator to prevent changes in the electric field E_{ind} which in turn, can disturb the droplet charge and stop the neutralisation.
The APs are inserted from the sides of the entire circumference through a kind of flat torus. This injection principle is based on the CLINCH experiment (CoLision Ice Nucleation Chamber, Ladino et al., 2011) which ensures a laminar flow and a great spatial APs mixture in the collision chamber inlet.

https://doi.org/10.5194/acp-2020-831
Preprint. Discussion started: 26 August 2020

Atmospheric Chemistry and Physics Discussions

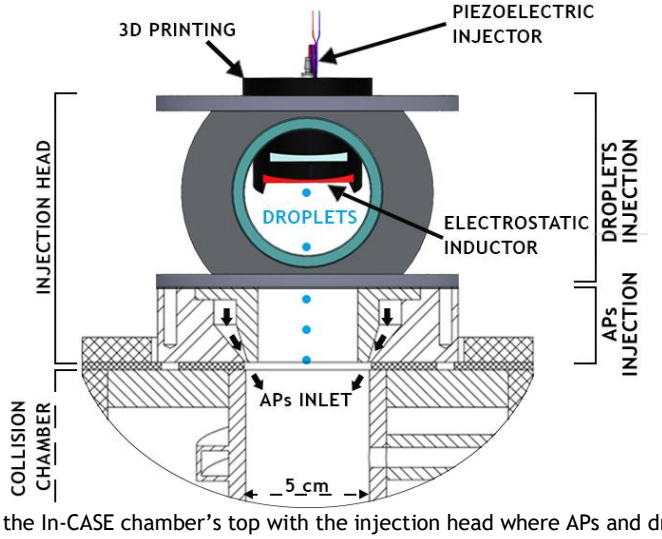

Figure 6 View of the In-CASE chamber's top with the injection head where APs and droplets are injected into the collision chamber.

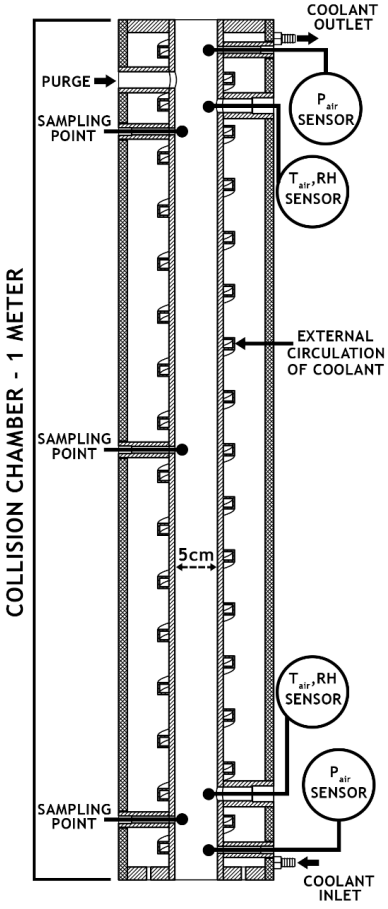

Figure 7 In-CASE collision chamber - 2D section plane.

https://doi.org/10.5194/acp-2020-831
Preprint. Discussion started: 26 August 2020

Atmospheric Chemistry and Physics Discussions

1.4.2 Collision chamber

The collision chamber is a one-meter stainless steel cylinder with an inner diameter of 5 cm (see Figure 7). The collision chamber's temperature is controlled through a coolant which spirally circulates outside the chamber, from the bottom to the top of the collision chamber. The pressure (P_{air}), temperature (T_{air}) and relative humidity (RH) are measured at the top and the bottom by sensors. To clean the chamber, water or compressed dried air are injected via a purge. Three sampling points are available but were not used for these experiments.
The temperature and the relative humidity discrepancies between top and bottom were respectively less than 1 °C and 4 % in all the CE measurements - the mean values are then considered for the both parameters.

1.4.2.1 Thermodynamic conditions

All the experiments were conducted at atmospheric pressure. To get comparable CE measurements, the temperature has been set to 0.58 ± 0.50 °C - as constant as possible between experiments. Three levels of relative humidity (RH) were considered - 71.1, 82.4 and 93.5 %. To increase the relative humidity at a given collision chamber temperature, the temperature of the pure water in the humidifier (Figure 2) was increased. The relative humidity level of 71.1 % was obtained by completely removing the humidifier to get the driest AP flow possible at the collision chamber inlet. At lab temperature (about 22 °C), the relative humidity of the dry AP flow ranged from 10 to 20 % at the In-CASE's chamber inlet.
Note that the AP flow before the injection head is also thermally set to inject APs with the same temperature as in the collision chamber.

1.4.2.2 Droplet evaporation

The change in droplet radius due to vaporisation in the collision chamber is calculated according to the section 13.2 of Pruppacher and Klett (1997). The corresponding terminal velocity is computed from Beard (1976). The residence time of the droplet in the chamber is computed considering these two changes. Since the droplet radius only decreases around 3 % by evaporation with the lower relative humidity considered in the experiments (71.1 %), the droplet evaporation in the collision chamber is neglected.

1.4.2.3 AP hygroscopicity

The APs are composed of pure sodium fluorescein salt which is a high hygroscopic chemical compound. The APs inside the collision chamber then grow to reach their equilibrium size with the relative humidity (RH). In order to evaluate the increase of size by humidification, the AP growth factor ($GroF$) measured in Quérel et al. (2014) was considered. The growth factor is defined as the ratio of the size of the humid AP over the size of the dry AP. Since their data are limited to relative humidity levels below 90 %, the kappa-theory described in Petters and Kreidenweis (2007) is used to extrapolate to the required values. To fit the measurements of Quérel et al. (2014) with the kappa-theory, only their data with a relative humidity level less than 85 % were considered. Figure 8 shows the AP growth factor related to the relative humidity for a kappa value of 0.23 and two extreme values of 0.2 and 0.27 - fitting to the sodium fluorescein salt hygroscopicity.
Thus, for relative humidity levels of 71.1 %, 82.4 % and 93.5 % studied here, a dry AP radius of 50 nm selected by the DMA grows with a growth factor ($GroF$) of 1.16, 1.27 and 1.57, respectively. Consequently, the CE measured are applied for size of respectively 58.0, 63.5 and 78.5 nm AP radii.
Note that the AP density is not the one of sodium fluorescein salt ($\rho_{fluorescein}$ = 1580 kg.m^{-3}) since APs contain water. Indeed, the water density (ρ_{water}) should be considered in the AP density (ρ_p) calculation. At a given relative humidity (RH), the AP density inside the chamber is then deduced by the equation (1):

$$\rho_p(RH) = \frac{\rho_{fluorescein} + \rho_{water} \times [GroF(RH)^3 - 1]}{GroF(RH)^3} \quad (1)$$

Since the relative humidity after the dryer (see Figure 2) ranges from 10 to 20 %, the AP growth factor is less than 1.02 (see Figure 8) in the DMA. APs are then considered dry when exiting the DMA.

https://doi.org/10.5194/acp-2020-831
Preprint. Discussion started: 26 August 2020

Atmospheric Chemistry and Physics Discussions

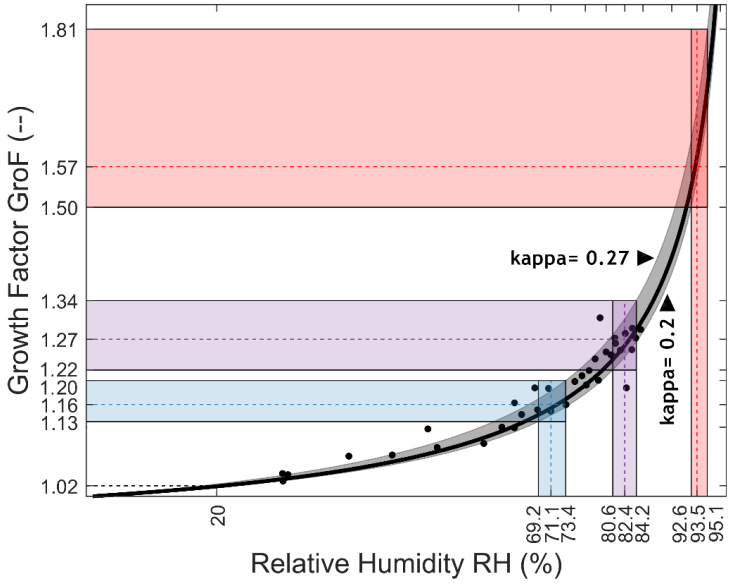

Figure 8 Growth factor ($GroF$) as function of the given relative humidity (RH). Data points (dots) from Quérel et al. (2014) and fittings (lines) with the kappa-theory (Petters and Kreidenweis, 2007).

1.4.3 In-CASE's bottom stage

The CE is calculated from the AP mass collected by the droplets during an experiment and the average AP mass concentration in the collision chamber. To obtain these quantities, the droplet train must be separated from the interstitial APs (which were not collected).

1.4.3.1 APs and droplets separation

The system developed to separate the droplet train from the AP flow is presented in Figure 9. It is composed of a converging portion (from 5 to 3 cm in diameter) where a gutter is inserted to prevent the water condensed on the wall from entering to the In-CASE's chamber bottom. The APs are directly vacuumed toward a HEPA filter (see Figure 2) at the upper part of the separator through four outlets while the droplets - containing collected APs - are impacted into a cup at the separator's lower part. To prevent AP pollution in the droplet impaction cup, a counter-flow is injected below the In-CASE's chamber and passes through the droplet impaction cup from nine holes set on its entire circumference. Since the counter-flow is injected at the laboratory temperature and the APs downward flow is colder, Argon - denser than the air - was selected to avoid any Rayleigh-Taylor instability (Sharp, 1983).
Argon is injected at 0.4 l/min. The diameter of the nine holes is 4 mm and the top of the droplet impaction cup is 2.5 cm. Thus, the upward Argon flow is injected at 5.9 and 1.4 cm/s, through the nine holes and the top of the impaction cup, respectively. Because the droplet velocity is about 25 cm/s (for the 50 µm droplet radius studied) and the AP terminal velocity is about 10^{-2} cm/s, APs can not settle into the impaction cup whereas droplets are impacted without undue disruption.

https://doi.org/10.5194/acp-2020-831
Preprint. Discussion started: 26 August 2020

Atmospheric Chemistry and Physics Discussions

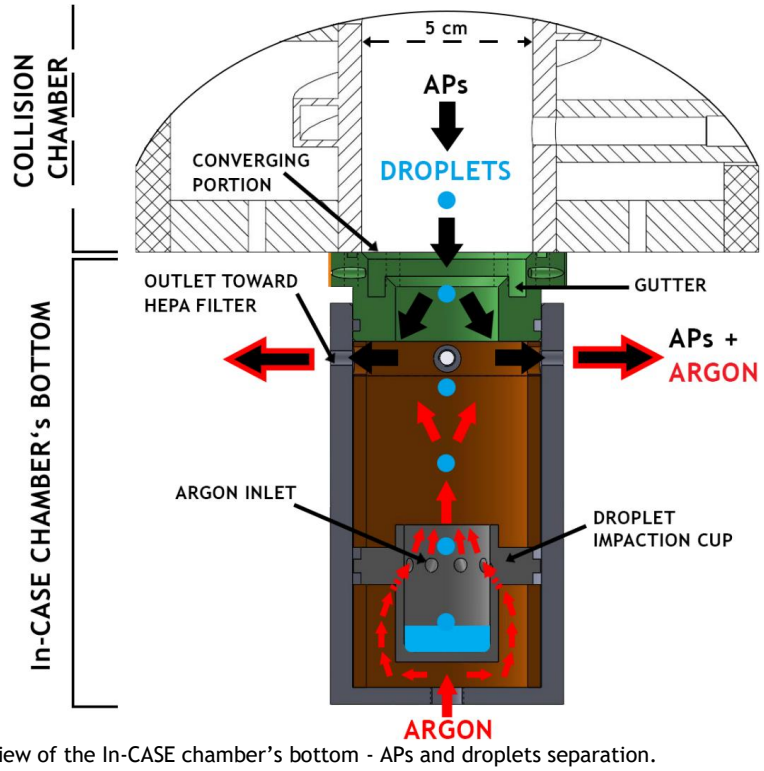

Figure 9 View of the In-CASE chamber's bottom - APs and droplets separation.

1.4.3.2 Validation

The droplets and APs separation were verified with two tests. First, In-CASE was run under usual experimental conditions except no droplets were generated. After five hours of experiment, a spectrometry analysis was performed in the droplet impaction cup and no fluorescein was detected. Thus, no AP had settled on the droplet impaction cup during the experiment.

The second test was to ensure that droplets were collected by the impaction cup. Then, In-CASE was again run like a typical experiment except the flow passing through the In-CASE chamber was clean air without any AP. Droplets were tracked by adding sodium fluorescein salt in the water supplying the piezoelectric injector. Since the concentration of sodium fluorescein salt in the water, the droplet generation frequency, the droplet size and the experiment time were known, the goal was to check if the expected fluorescein mass in the droplets and the actual measured fluorescein mass were equal. After five hours (= 450,000 injected droplets), a discrepancy of 2 % between expected and measured fluorescein mass was obtained. Therefore, all droplets are considered impacted in the impaction cup.

Finally, this indicates that the AP mass detected in the droplet impaction cup after an experiment results effectively from scavenging events in the In-CASE collision chamber.

https://doi.org/10.5194/acp-2020-831
Preprint. Discussion started: 26 August 2020

Atmospheric Chemistry and Physics Discussions

2 DATA ANALYSIS

2.1 Definition of the collection efficiency

At the end of an experiment, the collection efficiency (CE) is calculated from the equation (2):

$$CE(a, A, HR) = \frac{m_{AP,d}}{m_{AP,available}} \quad (2)$$

Where the AP mass collected by all droplets ($m_{AP,d}$) is directly measured by spectrometry analysis in the droplet impaction cup (see Figure 9) while the mass of available APs in the volume swept by the droplets ($m_{AP,available}$) is given by the equation (3) :

$$m_{AP,available} = \pi(A + GroF(RH) \times a)^2 \times F_d \times \Delta t \times H_{eff} \times C_{m,AP} \quad (3)$$

F_d and Δt are respectively the droplet generation frequency and the experiment duration - the product of those two quantities is the number of droplets injected during an experiment. Note that a is the AP dry radius corrected by the growth factor ($GroF$) which depends on the relative humidity (see section 1.4.2.3). H_{eff} is the effective height of interaction between droplets and APs. Since the APs are also falling in the In-CASE collision chamber, this height is not the In-CASE collision chamber's height ($H_{In-CASE}$) but is equal to the equation (4):

$$H_{eff} = \frac{U_{A,\infty}}{U_{A,\infty} + V_Q} H_{In-CASE} \quad (4)$$

However, as the droplet terminal velocity ($U_{A,\infty}$) is about 25 cm/s and the maximum AP flow velocity (V_Q) considered in the In-CASE collision chamber during the experiment is 5 mm/s (for an AP flowrate of 0.6 l/min), these both heights are thus considered equal ($H_{eff} \sim H_{In-CASE}$).

In equation (3), $C_{m,AP}$ is the mean AP mass concentration in the In-CASE collision chamber, estimated from the fluorescence spectrometry analysis of the HEPA filter though the equation (5):

$$C_{m,AP} = \frac{m_{AP,tot}}{\Delta t \times Q_{In-CASE,c}} \quad (5)$$

$Q_{In-CASE,c}$ is the AP flowrate within the In-CASE collision chamber.

2.2 DMA selection - multiple charged AP's principle

As previously stated, the AP flow travels through a DMA to select the particles according to their electrical mobility (Z) which is defined by the equation (6):

$$Z = \frac{n\, e\, Cu}{6\, \pi\, \eta_{air}\, a} \quad (6)$$

Where n, Cu, η_{air} are respectively the number of elementary charge (e), the Cunningham correction coefficient and the air dynamic viscosity (expressed here in poise).

Thus, for an AP radius selected by the DMA, all particles with the same $\frac{n\, Cu}{a}$ ratio are actually selected. For example, when an AP with a radius of 50 nm is selected (single charged), the AP radii of 75.8 nm (double charged) and 98.2 nm (triple charged) will also be selected and progress into the In-CASE collision chamber since they have the same electrical mobility. In this paper, "multiple charged APs" are referred as the APs with the same electrical mobility as the ones (single charged) selected by the DMA.

https://doi.org/10.5194/acp-2020-831
Preprint. Discussion started: 26 August 2020

Atmospheric Chemistry and Physics Discussions

At the DMA inlet, an aerodynamic impactor is placed to prevent the heaviest APs from entering into the DMA. Thus, for a given AP flowrate in the DMA, the multiple charged APs can be impacted at the DMA inlet and can then be neglected at the DMA outlet. To evaluate this case, the cut-off radius of the impactor at the DMA inlet must be considered (referred as $D_{50\%}/2$). This radius is defined as the one where 50 % of the APs are impacted. The Table 1 shows this parameter for every AP flowrate used during the experiment and for a given selected AP radius. The double charged AP radius with the same electrical mobility as the selected AP radius (single charged) is also indicated - when this latter size is large enough compared to the cut-off radius, it is assumed that there is no contribution of the multiple charged APs in the CE measurement. This is the case for a selected AP radius of 200 or 250 nm where the AP size distribution at the DMA outlet can be considered purely monodispersed.

However, for a selected AP radius of 50 or 150 nm, according to Table 1, the multiple charged AP radii cannot be neglected. Different experiments were run to perform a deconvolution of their respective contributions in the final CE calculation. This method is presented in Appendix A.

Table 1 AP selection parameters

Selected AP radius by the DMA (single charged)	Double charged AP radius with the same electrical mobility	AP flowrate in the DMA	Cut-off radius of the impactor at the DMA inlet ($D_{50\%}/2$)
$50\ nm$	$75.8\ nm$	$0.6\ l/min$	$213\ nm$
$150\ nm$	$253.7\ nm$	$0.6\ l/min$	$213\ nm$
$200\ nm$	$348.3\ nm$	$0.6\ l/min$	$213\ nm$
$250\ nm$	$444.3\ nm$	$0.4\ l/min$	$268.5\ nm$

2.3 Uncertainty evaluations

2.3.1 AP radius uncertainty

The first AP radius uncertainty is related to the AP selection by the DMA. Nevertheless, this uncertainty has been neglected since the spectral bandwidth of the DMA is quite small compared to the AP radius uncertainty addressed below.
Indeed, the only significant AP radius uncertainty results from the effective AP radius inside the In-CASE collision chamber due to the hygroscopicity of the APs. For the relative humidity levels studied (71.1, 82.4 or 93.5 %), the extreme relative humidity levels measured in all experiments are considered - for 71.1 %, the minimum and maximum values are 69.2 % and 73.4 %, respectively. As a reminder, the kappa-value is assumed from the Quérel et al. (2014) data and ranges from 0.2 to 0.27 (see Figure 8). The low uncertainty for the AP radius is then evaluated by considering the minimum growth factor ($GroF$) in Figure 8 for the lower level of relative humidity measured and the lower kappa value determined - respectively 69.2 % and 0.2. Similarly, for the same example (RH= 71.1 %), the high uncertainty for the AP radius is estimated by evaluating the maximum growth factor - for the maximum level of relative humidity observed and the maximum kappa value assumed - respectively 73.4 % and 0.27. In this example, for a dry AP radius of 50 nm selected by the DMA, its wet radius in the In-CASE collision chamber is likely to be 58 nm ($GroF$= 1.16) ranging from 56.5 nm ($GroF$= 1.13) to 60 nm ($GroF$= 1.20) resulting from the respective low and high uncertainties.

2.3.2 Uncertainty of the collection efficiency

Since the method of CE evaluation differs in the presence of multiple charged APs, the uncertainty calculation is also different depending on the situations. The method is described in the Appendix B.

When there are no multiple charged APs in the AP flow, the CE is directly estimated through the equation (3) which can be rewritten as the equation (7):

https://doi.org/10.5194/acp-2020-831
Preprint. Discussion started: 26 August 2020

Atmospheric Chemistry and Physics Discussions

$$CE(a, A, RH) = \frac{m_{AP,d}}{\pi(A+a)^2 \times N_d \times H_{eff} \times C_{m,AP}} \approx \frac{m_{AP,d}}{\pi A^2 \times N_d \times H_{In-CASE} \times C_{m,AP}} \quad (7)$$

Where N_d is the number of injected droplets during the experiment. The relative CE uncertainty (u_{CE}) is then evaluated according to Lira (2003) and summarised by the equation (8):

$$u_{CE} = \sqrt{{u_A}^2 + {u_{H_{In-CASE}}}^2 + {u_{N_d}}^2 + {u_{m_{AP,d}}}^2 + {u_{C_{m,AP}}}^2} \quad (8)$$

With:

- The relative uncertainty related to the droplet radius measurement (u_A) which is the ratio between the standard-deviation and the mean droplet radius on 200 pictures obtained by optical shadowgraphy. This relative uncertainty is about 1 %;
- The relative uncertainty of the In-CASE collision chamber's height ($u_{H_{In-CASE}}$) which is 1 %;
- The relative uncertainty of the number of droplets (u_{N_d}) which can be correlated to the droplet number effectively impacted on the droplet impaction cup. This relative uncertainty was evaluated during the validation of APs and droplet train separation (section 1.4.3.2) and is about 2 %;
- The relative uncertainty of the detected AP mass in the droplet impaction cup ($u_{m_{AP,d}}$) which takes into account the relative uncertainty related to the spectrometry analysis ($u_{fluorimeter}$) and the one caused by the dilution ($u_{dilution}$) - equation (9). Indeed, at the end of an experiment the water contained in the droplet impaction cup is dried and the residual AP mass is then dissolved in 2 ml volume of ammonia water.

$$u_{m_{AP,d}} = \sqrt{{u_{fluorimeter}}^2 + {u_{dilution}}^2} \quad (9)$$

  $u_{dilution}$ is estimated at 1 % meanwhile $u_{fluorimeter}$ is the main source of uncertainty. In fact, when the mass of AP collected by the droplet is close to the detection limit of the fluorimeter (about 10^{-15} kg in the droplet sample volume analyzed), $u_{fluorimeter}$ is up to 30 %.
- The relative uncertainty of the mean AP mass concentration in the In-CASE collision chamber ($u_{C_{m,AP}}$) which can be evaluated, according to the equation (5), by the equation (10):

$$\begin{cases} u_{C_{m,AP}} = \sqrt{{u_{m_{AP,tot}}}^2 + {u_{Q_{In-CASE,c}}}^2 + {u_{\Delta t}}^2} \approx \sqrt{{u_{m_{AP,tot}}}^2 + {u_{Q_{In-CASE,c}}}^2} \\ u_{m_{AP,tot}} = \sqrt{{u_{fluorimeter}}^2 + {u_{dilution}}^2} \end{cases} \quad (10)$$

  Where the relative uncertainty of the detected AP mass on the HEPA filter ($u_{m_{AP,tot}}$) depends on the one on the fluorimeter ($u_{fluorimeter}$) and the one on the dilution ($u_{dilution}$~1 %). In fact, the spectrometry analysis is performed by diluting the AP mass on the HEPA filter in a 100 ml ammonia water solution at the end of an experiment. The relative uncertainty of the AP flowrate in the In-CASE collision chamber ($u_{Q_{In-CASE,c}}$) is given by the datasheet of the constructor - about 1 %. Note that the relative uncertainty on the experiment time ($u_{\Delta t}$) is neglected since the error is approximately one second on a experiment that can last more than 5 hours.

3 RESULTS AND DISCUSSIONS

3.1 Extension of the Dépée et al. (2019) model

In all experiments, the droplet charge is 0 ± 600 elementary charges with a radius of about 50 µm. Since the AP charge distribution is similar to a Boltzmann distribution, an AP charge of more than 5 elementary charges is thus highly unlikely. Consequently, it is assumed that the contribution of the electrostatic forces on the CE is of second order and these effects were then neglected. Indeed, Dépée et al. (2019) numerically evaluated the contribution of the electrostatic forces on the CE for

https://doi.org/10.5194/acp-2020-831
Preprint. Discussion started: 26 August 2020

Atmospheric Chemistry and Physics Discussions

a droplet of 50 µm radius with 1000 elementary charges and 5 elementary charges on the AP. For these extreme values, they shown that the electrostatic forces increase the CE by a maximum of 42 % in the AP size range considered during the experiments (actually for an AP radius of 50 nm where the electrical mobility is the largest).

To extend the Dépée et al. (2019) model for the thermophoretic ($\boldsymbol{F_{th}}$) and diffusiophoretic forces ($\boldsymbol{F_{df}}$), the resulting velocity at the AP location ($\boldsymbol{U_{f@p}}^*$) given by the authors (in Equation 6) is replaced by the equation (11):

$$\boldsymbol{U}_{f@AP}{}^*(t) = \boldsymbol{U}_{f@AP}(t) + \frac{\tau_p}{m_p}\left(\boldsymbol{F_{buoy}} + \boldsymbol{F_{df}} + \boldsymbol{F_{th}}\right) \tag{11}$$

Where all the terms are defined in Dépée et al. (2019), except the thermophoresis and the diffusiophoresis which are given by Brock (1962) and Waldmann and Schmitt (1966), respectively, summarised in the Equations (12):

$$\begin{cases} \boldsymbol{F_{df}} = -6\pi\eta_{air}a\dfrac{0{,}74D_vM_{air}}{C_uM_{water}\rho_{air}} \times \overbrace{\dfrac{(\rho_{v,air}-\rho_{v,s})f_v}{Ar^{*2}}}^{①}\boldsymbol{u_r} \\ \boldsymbol{F_{th}} = -\dfrac{12\pi\eta_{air}a}{5P_{air}}\dfrac{(k_{air}+2{,}5k_{AP}K_n)k_{air}}{(1+3K_n)(2k_{air}+k_{AP}+5k_{AP}K_n)} \times \underbrace{\dfrac{(T_{air}-T_{d,s})f_h}{Ar^{*2}}}_{②}\boldsymbol{u_r} \end{cases} \tag{12}$$

With $\boldsymbol{u_r}$ - the unit vector in the radial direction from the droplet centre to the AP centre, r^* - the distance between the AP and droplet centres normalised by the droplet radius A, D_v - the diffusivity of vapor, K_n - the Knudsen number, M_{air} and M_{water} - the respective air and water molar masses, k_{air} and k_{AP} - the respective air and AP thermal conductivities. Note that the thermal conductivity of the sodium fluorescein salt is considered for k_{AP} - equal to 0.43 m.kg.s^{-3}.K^{-1} (Al-Azzawi et Owen, 1984).

In equations (12), the terms ① and ② represent the gradient of vapor density in the air and the thermal gradient, respectively. These two gradients are computed under the assumption that the temperature and vapor density profiles are spherically symmetric around the droplet (Wang et al., 1978). Because the droplet is falling in the air, f_v and f_h - which are the ventilation coefficient for the vapor and the heat respectively (Beard and Pruppacher, 1971) - correct the gradients since the profiles are actually disturbed by the airflow.

3.2 Collection efficiency measurements and analysis

In Figure 9, the CEs are presented for the three levels of relative humidity studied - 71.1, 82.4 and 93.5 % - and 6 dry AP radii ranging from 50 to 250 nm. As a reminder, all experiments were conducted with an air temperature of 0.58 ± 0.50°C at the atmospheric pressure, the AP charge distribution is similar to a Boltzmann distribution and the droplet charge is 0 ± 600 elementary charges. The droplet radius is 49.6 ± 1.3 µm. Note that the experimental conditions vary a little for the CE measurements at a given relative humidity level. On figure 9, the measurements are compared to computed efficiencies using the models described in Wang et al. (1978) (bottom) as well as the extended version of Dépée et al. (2019) (top). The envelopes are computed by considering the extreme conditions in all experiments - the droplet radius A, the relative humidity RH, the air temperature T_{air} - maximizing (dashed line) and minimizing (dotted line) the CE and the mean conditions (solid line). The experimental conditions presented in Figure 9 are summarised in Table 2. The wet AP radii are evaluated with the mean experimental conditions as well as the AP density (ρ_{AP}) which is calculated with (1). The CE measurements are summarised in Table 3.

Regarding the experimental results, it can be noted that the influence of the relative humidity via the thermophoresis and diffusiophoresis contribution on the CE is of first order. For the larger AP radii studied, the CE increases by a factor of 4 when the relative humidity passes from 93.5 to 71.1 % - filling up the Greenfield gap as the models predicts. A slight decline of the contribution of these two phoretic effects is observed when the AP radius decreases – the previous factor of 4 reducing to a factor of 3 for the smaller AP radii and for the same relative humidity range (from 93.5 to 71.1 %). Although this decrease is weak, it is in line with the theory. Indeed, when the AP radius decreases the contribution of the Brownian motion on the CE increases and starts dominating the

https://doi.org/10.5194/acp-2020-831
Preprint. Discussion started: 26 August 2020

Atmospheric Chemistry and Physics Discussions

thermophoretic and the diffusiophoretic forces. Consequently, the influence of the relative humidity on the CE is negligible for nanometric AP radii.

Moreover, the impact of the AP size is lower than the influence of the relative humidity for the experimental conditions considered. Indeed, between the larger and the smaller AP radii, the CE is only increased by a factor of 1.61, 1.59 and 2.03 for the respective relative humidity levels of 71.1, 82.4 and 93.5 %. A decrease of the AP size effect on the CE is noticeable when the thermophoresis and the diffusiophoresis contributions intensify - in other words when the relative humidity declines. This observation is in line with the modelling of the CE when a threshold is more and more visible as the relative humidity decreases, for the submicron AP radii studied.

Finally, for the AP sizes and the droplet radius studied, both models describe relatively well the observed CE variations when changing relative humidity. For the two lowest levels of relative humidity (71.1 and 82.4 %), the CE modelling is really close between both models since the thermophoresis and diffusiophoresis dominate the influence on the CE. Nevertheless, some significant discrepancies appear for the highest relative humidity (93.5 %), where the Dépée et al. (2019) extended model gives higher CE values. These differences result from the Wang et al. (1978) model which does not consider dynamic effects such as AP inertia, AP weight and interception, in contrast to the extended model of Dépée et al. (2019) which offers a complete description of the microphysical effects involved in-cloud.

Table 2 Mean experimental conditions (solid line) and extreme experimental conditions maximizing (dashed line) and minimizing (dotted line) the CE.

Line style	$A(\mu m)$	$RH(\%)$	$T(°C)$	$\rho_{AP}(kg.m^{-3})$
·····	50.4	95.1	0.75	1150
———	48.8	93.5	1.20	1150
– – – ·	47.6	92.6	1.60	1150
———	48.8	100.0	1.20	1150
·····	53.0	84.2	0.03	1282
———	50.8	82.4	0.27	1282
– – – ·	48.6	80.6	0.59	1282
– – – ·	50.8	100.0	0.27	1282
·····	50.6	73.4	0.14	1372
———	49.3	71.1	0.27	1372
– – – ·	48.0	69.2	0.37	1372
·····	49.3	100.0	0.27	1372

Table 3 CE measurements for the three levels of relative humidity (RH) and the wet AP radii (a). The droplet radius is 49.6 ± 1.3 µm.

$RH = 93.5\ \%$		$RH = 82.4\ \%$		$RH = 71.1\ \%$	
a (nm)	CE (--)	a (nm)	CE (--)	a (nm)	CE (--)
79	3.92×10^{-3}	64	7.15×10^{-3}	58	1.18×10^{-2}
119	2.98×10^{-3}	96	5.52×10^{-3}	88	1.12×10^{-2}
154	3.17×10^{-3}	125	5.16×10^{-3}	114	8.94×10^{-3}
235	2.48×10^{-3}	191	5.20×10^{-3}	174	8.50×10^{-3}
314	2.18×10^{-3}	254	4.69×10^{-3}	232	7.31×10^{-3}
393	1.93×10^{-3}	318	4.51×10^{-3}	290	7.32×10^{-3}

https://doi.org/10.5194/acp-2020-831
Preprint. Discussion started: 26 August 2020

Atmospheric Chemistry and Physics Discussions

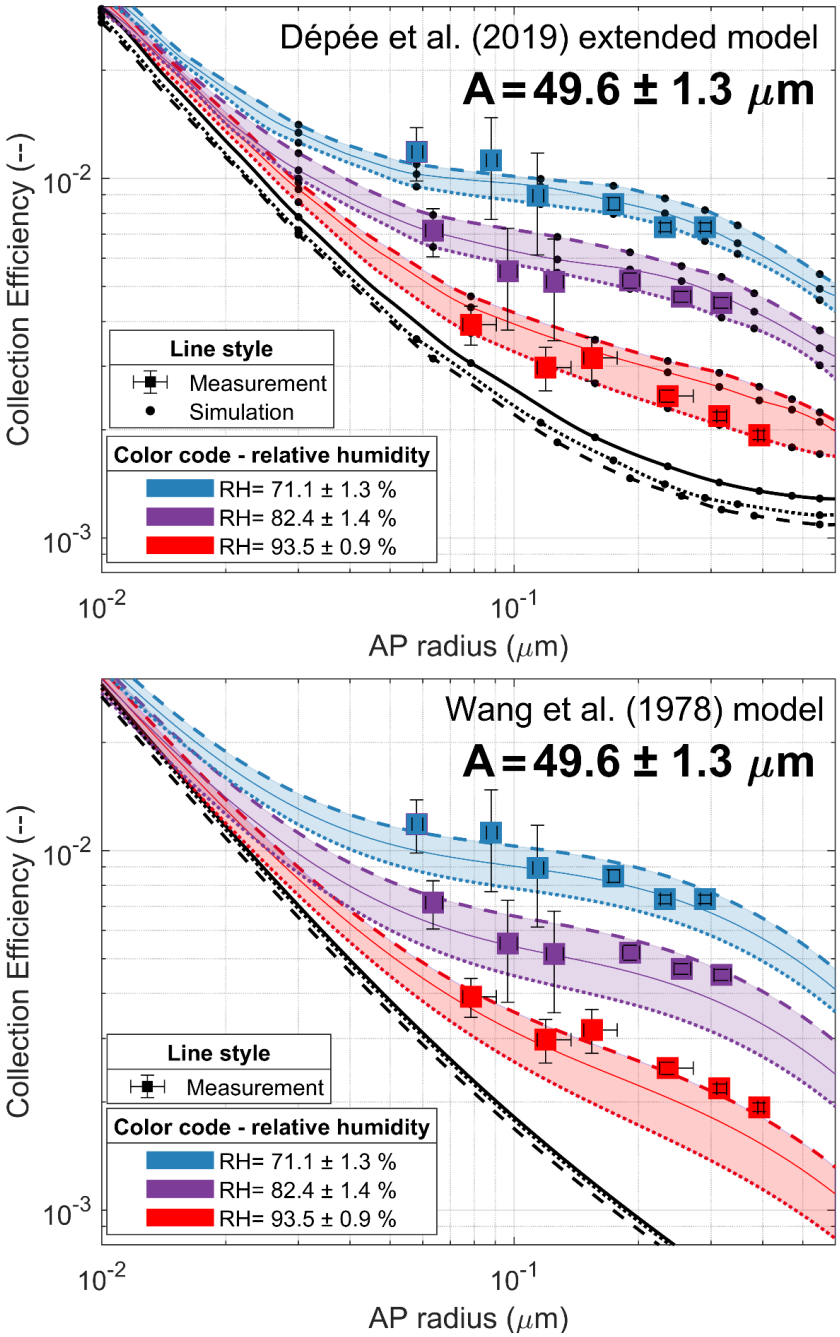

Figure 9 CE measurements for three levels of relative humidity - 71.1, 82.4 and 93.5 % - compared to the extended model of Dépée et al. (2019) (**top**) and the Wang et al. (1978) model (**bottom**). Squares are the CE measurements summarised in Table 3 while lines are the CE modelling resulting from the experimental conditions found in Table 2.

https://doi.org/10.5194/acp-2020-831
Preprint. Discussion started: 26 August 2020

Atmospheric Chemistry and Physics Discussions

CONCLUSIONS

In-CASE (In-Cloud Aerosol Scavenging Experiment) was built to conduct a set of experiments quantifying the contribution of any microphysics effects involved in the AP collection by falling cloud droplets. For this purpose, all parameters influencing the collection efficiency (CE) are controlled - i.e. the AP and droplet sizes, the AP and droplet electric charges and the relative humidity.

This study focused on the influence of relative humidity since the literature lacks baseline data validating the theoretical models of CE implemented in cloud, climate and pollution models. Indeed, only the work of Ardon-Dryer et al. (2015) is dedicated to check the CE variation for two levels of relative humidity and cloud droplet sizes ($A \leq$ 100 µm). Nevertheless, for the droplet radius considered, the authors conclude that the electrostatic forces could have played a key role on their CE measurements, since the AP and droplet are charged, however slightly.

In the new measured CE dataset that is presented here, the APs and droplets are neutralised. There is no significant remaining electrostatic effect considering the maximum residual AP and droplet charges for the droplet radius examined (A=49.6 ± 1.3 µm), twice larger than the one studied by Ardon-Dryer et al. (2015). Here, three levels of relative humidity were investigated - 71.1, 82.4 and 93.5 % which are typical in-cloud conditions.

From the measurements obtained, it is clear that the relative humidity - through the thermophoretic and diffusiophoretic forces - significantly impacts the CE. Indeed, an increase by a factor of 4 was observed for the CE when the relative humidity level declines from 93.5 to 71.1 %. Thus, it is quite important to consider these effects in cloud model since the levels of relative humidity are comparable from those used in this study. It was also shown that for the AP size considered in the present study, the impact of the AP size on the CE is a second order dependency. In fact, only a doubling of the CE was highlighted - for a relative humidity of 93.5 % - from the larger to the smaller AP radius considered. This impact of the AP size decreased when the influence of the relative humidity increases.

The CE computed with the well-established model of Wang et al. (1978) as well as the new Lagrangian model described in Dépée et al. (2019) and extended to phoretic effects were compared to the measurements. The agreement was good. Nevertheless, significant discrepancies between both models were revealed for high relative humiditiy (in a subsaturated air) where the relative humidity influence is weak. This can be attributed to the fact that the model of Wang et al. (1978) disregards some microphysics effects such as AP weight, AP inertia and interception which have a significant contribution near the Greenfield gap (Greenfield, 1957). Thus, the extended Lagrangian model of Dépée et al. (2019) offers a more appropriate estimation of the CE.

In this study, the electrostatic effects were not considered. However, Dépée et al. (2019) have shown an impact of several orders of magnitude on the CE, especially considering the electric charges of cloud droplets and radioactive APs. Then, it is essential to investigate the AP collection by clouds due to the electrostatic forces - referred as “electroscavenging”. Up to now, the analytical expression of the electrostatic forces - based on the image charge theory developed by Jackson (1999) - has never been experimentally validated or at least emphasised. Consequently, In-CASE was also used to study the influence of the droplet and AP charge on CE which is addressed in a second paper (**Dépée et al., 2020**).

https://doi.org/10.5194/acp-2020-831
Preprint. Discussion started: 26 August 2020

Atmospheric Chemistry and Physics Discussions

Appendix A - Evaluation method of the collection efficiency in the presence of multiple charged APs

This appendix presents the method used to evaluate the CE when the selected AP radius by the DMA is 50 or 150 nm - when the multiple charged APs can not be neglected (see section 2.2).

A.1 Ratio of multiple charged APs

A.1.1 Selected AP radius of 50 nm

Before the AP selection, the DMA charges the APs following a known charging law (Wiedensohler, 1988) with an energy X-ray neutraliser (not presented in Figure 2).

The first step is to estimate the number and mass ratios of multiple charged APs in the mean AP mass concentration measured in the In-CASE collision chamber ($C_{m,AP}$). For this purpose, the size distribution of the APs produced by the atomiser is measured just before the DMA selection (Figure 3). The AP number concentration at the single (50 nm), double (75.8 nm), triple (98.2 nm), quadruple (119.1 nm) and quintuple (139.1 nm) charged radii are deduced from the size distribution.

Those AP number concentrations are the total concentrations at a given multiple charged AP radius. From those total concentrations, a fraction will be actually carrying the correct charge number to have the exact electrical mobility selected by the DMA (1 charge for 50 nm, 2 charge for 75.8 nm, 3 charges for 98.2 nm, etc.). This fraction number ($F_{N,n}$) of an AP radius (a) carrying n elementary charge(s) can be estimated through the APs charging law imposed by the energy X-ray neutraliser - defined by Wiedensohler (1988). This similar Boltzmann distribution is defined in the equations (13):

$$\begin{cases} F_{N,n}(a) = 10^{\left[\sum_{i=1}^{6} c_i(n)\left(log\left(\frac{2a}{10^{-9}}\right)\right)^{i-1}\right]} & if\ n < 3 \\ F_{N,n}(a) = \frac{e}{\sqrt{8\pi^2\varepsilon_0 a k_b T_{air}}} exp^{-\frac{\left[n-\frac{4\pi\varepsilon_0 a k_b T_{air}}{e^2} ln\left(\frac{Z_{i+}}{Z_{i-}}\right)\right]^2}{2\frac{4\pi\varepsilon_0 a k_b T_{air}}{e^2}}} & if\ n \geq 3 \end{cases} \quad \begin{cases} c_{i\in[1,6]}(1) = \begin{bmatrix} -2{,}3484 \\ 0{,}6044 \\ 0{,}4800 \\ 0{,}0013 \\ -0{,}1553 \\ 0{,}0320 \end{bmatrix} \\ c_{i\in[1,6]}(2) = \begin{bmatrix} -44{,}4756 \\ 79{,}3772 \\ -62{,}8900 \\ 26{,}4492 \\ -5{,}7480 \\ 0{,}5049 \end{bmatrix} \end{cases} \tag{13}$$

Where ε_0, k_b and T_{air}≈295.15 K are the vacuum permittivity, the Boltzmann's constant and the lab temperature. The ion mobility ratio ($\frac{Z_{i+}}{Z_{i-}}$) is assumed to be equal to 0.875 (Wiedensohler,1988).

Finally, the effective AP numbers for the respective multiple charged AP radii have been evaluated in the AP flow at the DMA's outlet (corresponding to the AP flow going into the In-CASE collision chamber). Thus, the mass fractions ($F_{m,n}$) for the single, double…, quintuple charged AP radii were estimated. It was found that the quadruple and quintuple charged AP radii can be neglected since their weight less than 6 % in the mean AP mass concentration in the In-CASE collision chamber ($C_{m,AP}$). Moreover, since their number concentrations are really poor (less than 50 cm^{-3}) compared to the

https://doi.org/10.5194/acp-2020-831
Preprint. Discussion started: 26 August 2020

Atmospheric Chemistry and Physics Discussions

single, double and triple charged radius (~10^3-10^4 cm^{-3}), the likelihood of those APs to be collected by a droplet in the collision chamber is extremely unlikely.

A.1.2 Selected AP radius of 150 nm

For a selected AP radius of 150 nm, only the double charged APs are considered since the triple charged APs are assumed to be stopped by the impactor at the DMA inlet (triple charged radius = 353.4 nm and $D_{50\%}/2$= 213 nm, Table 1). The mass fractions ($F_{m,n}$) of the single and double charged are evaluated in the same way as a 50 nm selected AP radius.

A.2 Deduction of the collection efficiency

A.2.1 Selected AP radius of 50 nm

As explained in section 2.2, when the selected AP radius by the DMA is 50 nm, the AP mass collected at the In-CASE's chamber bottom ($m_{AP,d}$) is actually the sum of the masses of the single (50 nm), double (75.8 nm) and triple (98.2 nm) charged AP collected by the droplet train. This can also be defined as the linear combination of the collection efficiencies ($CE_i(a_i, A, RH)$) and the available AP mass in the volume swept by the droplets ($m_{AP,available}(a_i)$) at a given multiple charged dry AP radius (a_i) - equation (14):

$$m_{AP,d} = m_{50\,nm,d} + m_{75.8\,nm,d} + m_{98.2\,nm,d} = \sum_{i=1}^{3} CE_i(a_i, A, RH) \times m_{AP,available}(a_i) \quad (14)$$

Where the respective available AP masses in the volume swept by the droplets are defined by the equation (15):

$$m_{AP,available}(a_i) = \pi(A + GroF(RH) \times a_i)^2 \times F_d \times \Delta t \times H_{eff} \times C_{m,AP} \times F_{m,n}(a_i) \quad (15)$$

All the parameters given in equation (8) are either measured or initially known, except the collection efficiencies (CE_i) for the single, double and triple charged AP dry radius. To deduce those three unknown parameters, a set of j linearly independent experiments ($j \geq 3$) has been performed by varying the ratio of the multiple charged APs (by changing the AP size distribution mode in Figure 3). The matrix system is then described through the equation (16):

$$M_{collected\ mass} = M_{available} \otimes M_{CE} \quad (16)$$

Where the one-dimension matrix of the collected mass ($M_{collected\ mass}$) for the set of j experiment is noted as the equation (17):

$$M_{collected\ mass} = \begin{bmatrix} m_{AP,d,1} \\ \vdots \\ m_{AP,d,j} \end{bmatrix} \quad (17)$$

The two-dimension matrix of the available AP masses in the volume swept by the droplet ($M_{available}$) for the single (a_1), double (a_2) and triple (a_3) charged is defined as the equation (18):

$$M_{available} = \begin{bmatrix} m_{AP,available,1}(a_1) & m_{AP,available,1}(a_2) & m_{AP,available,1}(a_3) \\ \vdots & \vdots & \vdots \\ m_{AP,available,j}(a_1) & m_{AP,available,j}(a_2) & m_{AP,available,j}(a_3) \end{bmatrix} \quad (18)$$

The one-dimension matrix containing all the unknow CEs (M_{CE}) is the equation (19):

$$M_{CE} = \begin{bmatrix} CE_1 \\ CE_2 \\ CE_3 \end{bmatrix} \quad (19)$$

Finally, this matrix system (16) is numerically solved by the quasi-Newton method. The uniqueness of the solution was verified - the initial value was changed in the solving method, giving the same solution vector.

https://doi.org/10.5194/acp-2020-831
Preprint. Discussion started: 26 August 2020

Atmospheric Chemistry and Physics Discussions

752 A.2.2 Selected AP radius of 150 nm
753
754 Like the same principle as before, the AP mass collected by the whole droplets ($m_{AP,d}$) is the linear
755 combination of the single (150 nm) and double charged (253.7 nm), defined as the equation (20):

$$m_{AP,d} = m_{150\ nm,d} + m_{253.7\ nm,d} = \sum_{i=1}^{2} CE_i(a_i, A, RH) \times m_{AP,available}(a_i) \quad (20)$$

756
757 Nevertheless, to avoid additional experiments and numerically reverse a similar matrix system as
758 (10), it was assumed that the CE of a dry AP radius of 253.7 nm is equivalent to the one for a dry AP
759 radius of 250 nm. Then, the CE for a 150 nm dry AP radius is deduced by the equation (21):

$$\begin{aligned} CE_1(150\ \text{nm}, A, RH) &= \frac{m_{AP,d} - CE_2(253.7\ nm, A, RH) \times m_{AP,available}(253.7\ nm)}{m_{AP,available}(150\ \text{nm})} \\ &\approx \frac{m_{AP,d} - CE(250\ nm, A, RH) \times m_{AP,available}(253.7\ nm)}{m_{AP,available}(150\ \text{nm})} \end{aligned} \quad (21)$$

760
761 The right term in equation (21) has no unknown since the CE of a 250 dry AP radius
762 ($CE_2(250\ nm, A, RH)$) has been previously calculated with the method developed in section 2.1.
763
764
765
766
767
768
769
770
771
772
773
774
775
776
777
778
779
780
781
782
783
784
785
786
787
788
789
790
791
792
793
794
795
796
797
798
799
800

https://doi.org/10.5194/acp-2020-831
Preprint. Discussion started: 26 August 2020

Atmospheric Chemistry and Physics Discussions

Appendix B - Uncertainty of the collection efficiency in the presence of multiple charged APs

This appendix presents the method used to evaluate the CE uncertainty when the selected AP radius by the DMA is 50 or 150 nm - when the multiple charged APs can not be neglected (see section 2.2).

B.1 With a selected dry AP radius of 150 nm

Since the CE of a selected dry AP radius of 150 nm ($CE(150\ \mathrm{nm}, \mathrm{A}, RH)$) is calculated through the CE of a selected dry AP radius of 250 nm ($CE(250\ \mathrm{nm}, \mathrm{A}, RH)$) - equation (21) - the uncertainty on the CE for the 150 nm ($u_{CE(150\ \mathrm{nm},\mathrm{A},RH)}$) is evaluated by propagating the uncertainty on the CE for 250 nm ($u_{CE(250\ \mathrm{nm},\mathrm{A},RH)}$). It means the term $u_{CE(250\ \mathrm{nm},\mathrm{A},HR)}$ is added in equation (8) to deduce $u_{CE(150\ \mathrm{nm},\mathrm{A},HR)}$.

B.2 With a selected dry AP radius of 50 nm

When the selected dry AP radius is 50 nm, the matrix system (16), solved by a quasi-Newton method, is composed of parameters each with their relative uncertainties. The relative CE uncertainties of the single (50 nm), double (75.8 nm) and triple (98.2 nm) charged dry AP radius are then deduced by randomly perturbing the terms of the matrix $M_{collected\ mass}$ and $M_{available}$ in equation (16) within the limits of their respective experimental relative uncertainties. 10,000 perturbed matrix systems were generated by the Monte-Carlo method and solved with the quasi-Newton method. From the 10,000 solution vectors - shaped like the equation (17) - the ones with negative CEs were removed since they have no physical meaning. The Figure 10 shows the set of the solutions for a relative humidity level of 71.1 % and a single charged dry AP radius (50 nm).
Finally, the relative uncertainty of the CE is given by the standard deviation (σ) of the solution distribution.

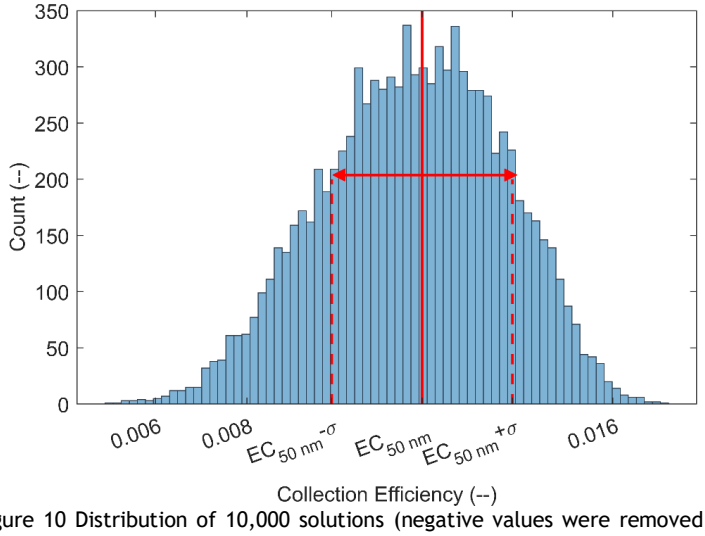

Figure 10 Distribution of 10,000 solutions (negative values were removed) for a relative humidity level of 71.1 % and a single charged dry AP radius (50 nm)

https://doi.org/10.5194/acp-2020-831
Preprint. Discussion started: 26 August 2020

Atmospheric Chemistry and Physics Discussions

References

Adachi, K., Kajino, M., Zaizen, Y., & Igarashi, Y. (2013). Emission of spherical cesium-bearing particles from an early stage of the Fukushima nuclear accident. *Scientific reports*, *3*, 2554.

Al-Azzawi, H. K., & Owen, I. (1984). Measuring the thermal conducitivity of uranin. *International journal of heat and fluid flow*, *5*(1), 57-59.

Ardon-Dryer, K., Huang, Y. W., & Cziczo, D. J. (2015). Laboratory studies of collection efficiency of sub-micrometer aerosol particles by cloud droplets on a single-droplet basis. *Atmospheric Chemistry and Physics*, *15*(16), 9159-9171.

Beard, K. V., & Pruppacher, H. R. (1971). A wind tunnel investigation of the rate of evaporation of small water drops falling at terminal velocity in air. *Journal of the atmospheric Sciences*, *28*(8), 1455-1464.

Beard, K. V. (1976). Terminal velocity and shape of cloud and precipitation drops aloft. *Journal of the Atmospheric Sciences*, *33*(5), 851-864.

Bell, M. L., Davis, D. L., & Fletcher, T. (2004). A retrospective assessment of mortality from the London smog episode of 1952: the role of influenza and pollution. *Environmental health perspectives*, *112*(1), 6-8.

Brock, J. R. (1962). On the theory of thermal forces acting on aerosol particles. *Journal of Colloid Science*, 17(8), 768-780.

Dépée, A., Lemaitre, P., Gelain, T., Mathieu, A., Monier, M., & Flossmann, A. (2019). Theoretical study of aerosol particle electroscavenging by clouds. *Journal of Aerosol Science*, *135*, 1-20.

Dépée, A., Lemaitre, P., Gelain, T., Monier, M., & Flossmann, A. (2019). Laboratory study of the collection efficiency of submicron aerosol particles by cloud droplets. Part II - Influence of electric charges.

Devell, L., Tovedal, H., Bergström, U., Appelgren, A., Chyssler, J., & Andersson, L. (1986). Initial observations of fallout from the reactor accident at Chernobyl. *Nature*, *321*(6067), 192-193.

Flossmann, A. I., Hall, W. D., & Pruppacher, H. R. (1985). A theoretical study of the wet removal of atmospheric pollutants. Part I: The redistribution of aerosol particles captured through nucleation and impaction scavenging by growing cloud drops. *Journal of the Atmospheric Sciences*, *42*(6), 583-606.

Flossmann, A. I. (1998). Interaction of aerosol particles and clouds. *Journal of the atmospheric sciences*, *55*(5), 879-887.

Greenfield, S. M. (1957). Rain scavenging of radioactive particulate matter from the atmosphere. *Journal of Meteorology*, *14*(2), 115-125.

Jackson, J. D. (1999). Classical electrodynamics.

Jaenicke, R. (1993). Tropospheric aerosols. In *International Geophysics* (Vol. 54, pp. 1-31). Academic Press.

Jost, D. T., Gäggeler, H. W., Baltensperger, U., Zinder, B., & Haller, P. (1986). Chernobyl fallout in size-fractionated aerosol. *Nature*, *324*(6092), 22-23.

Kaneyasu, N., Ohashi, H., Suzuki, F., Okuda, T., & Ikemori, F. (2012). Sulfate aerosol as a potential transport medium of radiocesium from the Fukushima nuclear accident. *Environmental science & technology*, *46*(11), 5720-5726.

Ladino, L., Stetzer, O., Hattendorf, B., Günther, D., Croft, B., & Lohmann, U. (2011). Experimental study of collection efficiencies between submicron aerosols and cloud droplets. *Journal of the Atmospheric Sciences*, *68*(9), 1853-1864.

https://doi.org/10.5194/acp-2020-831
Preprint. Discussion started: 26 August 2020

Laguionie, P., Roupsard, P., Maro, D., Solier, L., Rozet, M., Hébert, D., & Connan, O. (2014). Simultaneous quantification of the contributions of dry, washout and rainout deposition to the total deposition of particle-bound 7Be and 210Pb on an urban catchment area on a monthly scale. *Journal of Aerosol Science*, *77*, 67-84.

Lira, I. (2003). Evaluating the measurement uncertainty: fundamentals and practical guidance.

Petters, M. D., & Kreidenweis, S. M. (2007). A single parameter representation of hygroscopic growth and cloud condensation nucleus activity. *Atmospheric Chemistry and Physics*, *7*(8), 1961-1971.

Pöllänen, R., Valkama, I., & Toivonen, H. (1997). Transport of radioactive particles from the Chernobyl accident. *Atmospheric Environment*, *31*(21), 3575-3590.

Pruppacher, H. R., & Klett, J. D. (1997). *Microphysics of Clouds and Precipitation.* (Dordrecht/Boston/London).

Quérel, A., Lemaitre, P., Monier, M., Porcheron, E., Flossmann, A. I., & Hervo, M. (2014). An experiment to measure raindrop collection efficiencies: influence of rear capture. *Atmospheric Measurement Techniques*, *7*(5), 1321-1330.

Reischl, G. P. W. W., John, W., & Devor, W. (1977). Uniform electrical charging of monodisperse aerosols. *Journal of Aerosol Science*, *8*(1), 55-65.

Santachiara, G., Prodi, F., & Belosi, F. (2012). A review of termo-and diffusio-phoresis in the atmospheric aerosol scavenging process. Part 1: Drop scavenging. *Atmospheric and Climate Sciences*, *2*(02), 148.

Sharp, D. H. (1983). *Overview of Rayleigh-taylor instability* (No. LA-UR-83-2130; CONF-8305110-2). Los Alamos National Lab., NM (USA).

Tao, W. K., Chen, J. P., Li, Z., Wang, C., & Zhang, C. (2012). Impact of aerosols on convective clouds and precipitation. *Reviews of Geophysics*, *50*(2).

Tinsley, B. A., Zhou, L., & Plemmons, A. (2006). Changes in scavenging of particles by droplets due to weak electrification in clouds. *Atmospheric Research*, *79*(3-4), 266-295.

Tinsley, B. A., & Zhou, L. (2015). Parameterization of aerosol scavenging due to atmospheric ionization. *Journal of Geophysical Research: Atmospheres*, *120*(16), 8389-8410.

Twomey, S. (1974). Pollution and the planetary albedo. *Atmospheric Environment (1967)*, *8*(12), 1251-1256.

Waldmann, L., & Schmitt, K. H. (1966). Thermo-phoresis and diffusiophoresis of aerosols. *Aerosol Science*, 137-162.

Wang, P. K., Grover, S. N., & Pruppacher, H. R. (1978). On the effect of electric charges on the scavenging of aerosol particles by clouds and small raindrops. *Journal of the Atmospheric Sciences*, *35*(9), 1735-1743.

Wiedensohler, A. (1988). An approximation of the bipolar charge distribution for particles in the submicron size range. *Journal of Aerosol Science*, *19*(3), 387-389.